Capacity Analysis for Optical Wireless Communication With Non-Monotonic Receiver Nonlinearity

Tianrui Lin, Jingyin Tang, Qingqing Hu, Nuo Huang, and Chen Gong, *Senior Member, IEEE*

***Abstract*—In this work, we develop a theoretical transmission model for optical wireless communication systems with receiver nonlinearity. To provide a framework for analyzing transmission rates, we derive lower and upper bounds on channel capacity under average and peak optical power constraints in both single-input single-output and multiple-input multiple-output systems using entropy power inequalities and dual expression. Numerical results verify the tightness of our derived capacity bounds and highlight the significant relationship between channel capacity and receiver nonlinearity.**

***Index Terms*—Channel capacity, receiver nonlinearity, optical wireless communication.**

I. Introduction

The development of wireless communication focuses on higher efficiency and reliability, thereby enabling seamless connectivity and enhanced user experiences [1]. Optical wireless communications (OWC) is a unique alternative to traditional radio frequency (RF) communications. It offers expanded spectrum resources, heightened security, and additional capabilities such as indoor positioning and navigation. Notably, OWC is recognized for its eco-friendliness and energy efficiency [2], [3], positioning it as an emerging pivotal technology in the communication landscape. Shannon Theorem lays down a theoretical framework for determining the maximum achievable data rate of a linear channel with a specified bandwidth and noise power spectral density without transmission errors [4]. However, despite the theoretical results available for RF communications, the extension to OWC needs further endeavor. The discrepancy stems from the unique attributes of OWC, including its dual role in communication and illumination, specific modulation and detection needs, and a different occupied spectral domain and modulation scheme from RF communication. Moreover, in wireless RF communication systems, the power amplifiers at the RF transmitter introduce nonlinear distortion, especially when operating near the maximum power, leading to saturation. However, in OWC, the nonlinearities are most significant at the receiver side, where photodetectors (such as photodiodes or avalanche photodiodes (APDs)) can exhibit nonlinear behavior under high optical power levels, leading to saturation and signal distortion during the optical-to-electrical conversion.

This work was supported by National Natural Science Foundation of China under Grant 62331024, Grant 62171428 and Grant 62101526.

The authors are with the CAS Key Laboratory of Wireless-Optical Communications, University of Science and Technology of China, Hefei, Anhui 230027, China (e-mail: trlin@mail.ustc.edu.cn; tangjy27@mail.ustc.edu.cn; ruixihu@mail.ustc.edu.cn; huangnuo@ustc.edu.cn; cgong821@ustc.edu.cn).

Additionally, there are specific safety standards that OWC must adhere to, including avoiding excessive optical intensity to prevent harm to the eyes and skin.

Given the luminous capability of light-emitting diode (LED) and laser diode (LD), there is also a maximum allowable optical intensity. A range of studies has delved into the capacity of discrete [5]–[8] and continuous-time Poisson channels [9]–[11]. Furthermore, Gaussian model often allows for simpler analysis and mathematical calculations compared to the Poisson model. The capacity of Gaussian model with input-dependent noise has been studied in [12]–[14]. Moreover, other studies have specifically targeted multiple-input multiple-output (MIMO) systems [15], [16].

The nonlinearity, primarily stemming from hardware imperfections in optical sources, photodetectors, and auxiliary electronic circuits, can induce extra distortion. These imperfections can lead to various issues including harmonic generation, saturable absorption, self-phase modulation, intermodulation distortion, quantization discrepancies and clipping aberrations. From the perspective of the communications field, such nonlinearity detrimentally impact the bit error rate (BER), degrading not only the primary system but also neighboring systems within the spectral range. To evaluate the impact of nonlinearity on the performance of a communication system, it is essential to conduct comprehensive modeling and analysis. This includes mathematical representations of the nonlinearities, simulations, and empirical tests. Numerous studies aim to investigate the performance issues associated with nonlinearity, addressing challenges such as out-of-band radiation and envelope limiting [17]–[19]. These works also emphasize the importance of preventing signals from operating in a device nonlinear region by avoiding significant power fluctuations. For MIMO systems, work [20] investigated nonlinear amplitude distortion, deriving an accurate upper bound on the BER for zero-forcing receivers with quadrature amplitude modulation amid channel estimation error. The lower and upper bounds for fading MIMO channel based on a general transmission model have been studied in [21]. In multicarrier systems, the varied amplitudes and phases of individual subcarriers result in larger nonlinear distortions. Such variations can lead to phenomena like intermodulation products, spectral regrowth and other nonlinear effects. Several studies have delved into the potential of multicarrier systems affected by transmitter clipping [22] and the capacity of orthogonal frequency division multiplexing (OFDM) channels under high peak-to-average power ratios [23], [24]. To combat

the distortions induced by nonlinearity, technologies such as pre-distortion, digital signal processing, and adaptive power control have been developed [25], [26].

Despite existing research, one area that remains relatively unexplored is the receiver nonlinearity in OWC systems, especially under high levels of background radiation or signal strength. In addition, the lack of a comprehensive analytical framework for nonlinear systems complicates the assessment of nonlinearity impact on channel capacity.

In this work, we investigate the capacity bounds for OWC with non-monotonic receiver nonlinearity. Taking into account the channel state, nonlinear function and thermal noise, we develop a theoretical transmission model for OWC with receiver nonlinearity. To provide a framework for analyzing the transmission rate, we derive lower and upper bounds on the channel capacity under average power constraint and peak power constraint in single-input single-output (SISO) and MIMO system, using entropy power inequality (EPI) and well-designed dual expressions. We derive these bounds under the assumption that the channel matrix is perfectly known at the transmitter. To evaluate the capacity reduction due to nonlinearity in a practical scenarios, we consider several representative nonlinear models in OWC. Numerical results demonstrate the tightness of the derived capacity bounds and highlight the significant relationship between channel capacity and receiver nonlinearity. These comparisons provide deeper insights into how nonlinearity at the receiver affects the overall system performance at high power levels.

The paper is organized as follows. The nonlinear receiver OWC system model is described in Section II. Sections III and IV derive the lower and upper capacity bounds for SISO and MIMO systems, respectively. Section V provides numerical results of lower and upper bounds for several nonlinear models. Finally, Section VI concludes this work.

II. Channel Model

The photodetector, such as photodiode, APD, and single-photon avalanche diode, as well as analog-to-digital converters (ADCs) and low-noise amplifier (LNA), typically exhibit nonlinearity [27], [28]. From the communication perspective, nonlinearity effects lead to performance degradation, affecting not only the system itself but also neighboring systems operating within the same contaminated spectral range. Such nonlinear relationship may be non-monotonic [29]–[32].

As illustrated in Fig. 1(a), we consider an OWC system with intensity-modulation and direct-detection (IM/DD). At the transmitter, the driving circuit drives the light source with an electrical signal to emit an optical signal. The receiver-side front-end photodetector converts the detected optical signal into an electrical signal which is fed into the backend processing circuit for data recovery.

Figure 1(b) shows the experimental setup of an OWC system. The transmitter-side nonlinearity is caused by devices such as high-power amplifier, LNA, or LED. Assume that the transmitter has accurate knowledge of its own nonlinearity characteristics. Figure 1(c) shows the nonlinear relationship between the incident optical power and the output of the APD. Consider a memoryless nonlinear receiver system characterized by nonlinear function $y = \phi(x)$. Assume that the mapping $y = \phi(x)$ is not necessarily one-to-one, and is a Borel function, i.e., for any y, set $\{\phi(x) \leqslant y\}$ consists of the union and intersection of a countable number of intervals. Such assumption preserves the measurable properties of signal. Moreover, assume that the probability of $\{\phi(x) = \pm\infty\}$ is zero.

The general transmission model for a nonlinear receiver is given by

$$R(t) = \phi(H(t) X(t)) + n(t), \tag{1}$$

where $X(t)$ and $R(t)$ are the transmitted signal and received signal, respectively; $H(t)$ denotes the channel link gain; $\phi(\cdot)$ denotes the memoryless time-invariant nonlinearity function, and $n(t)$ denotes the zero-mean Gaussian noise with variance σ^2. Based on Gaussian assumption, we can effectively obtain tractable forms of the upper and lower bounds to evaluate capacity, which would otherwise be difficult or impossible to derive analytically with more complicated noise models. Note that the nonlinearity at the receiver is predominantly triggered

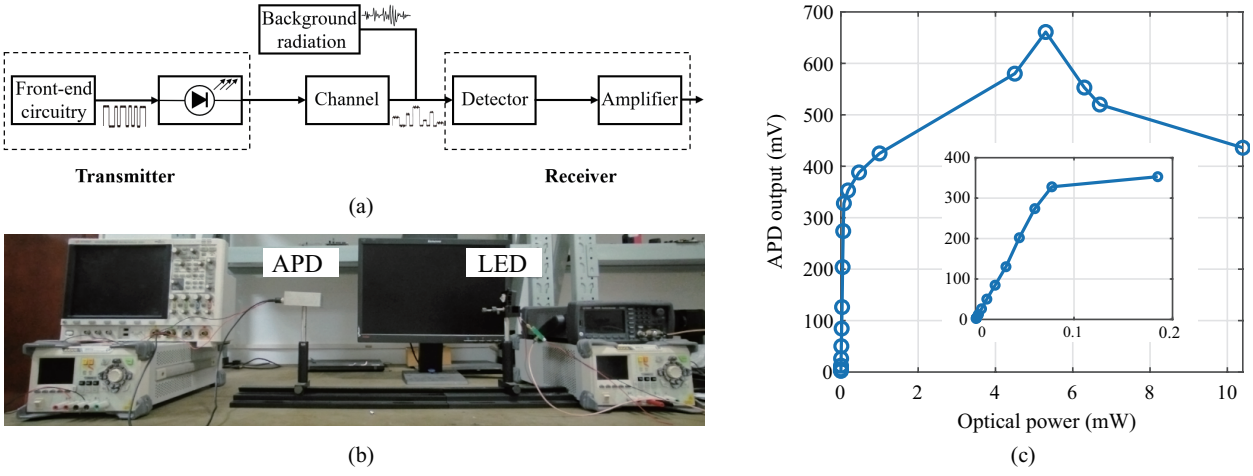

Fig. 1. (a) A representative OWC system. (b) The experimental setup for OWC system. (c) The APD output versus incident optical power.

by the high-power signal, while the effect of noise is relatively small. The nonlinear function $\phi(\cdot)$ is illustrated in Fig. 2. For typical physical devices, the "flat" region generally occurs in the saturation region when the input power is too high. For example, when the nonlinear function is a hard clipping function, all values of the received signal exceeding the hard clipping threshold will be limited to the threshold.

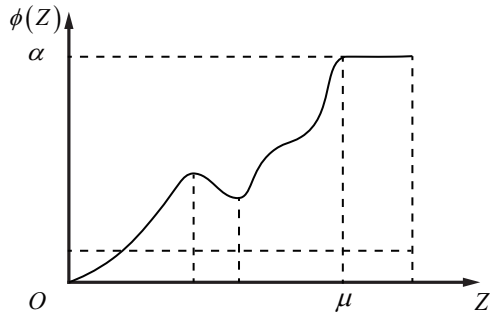

Fig. 2. Nonlinearity "input-output" function in receiver.

Here, the independent variable Z is constrained to the range $[0, \mu]$, where $\mu = HA$. The function $\phi(Z)$ for $Z \in [0, \mu]$ is constrained to the range $[0, \alpha]$.

We consider the following average and peak optical power constraints,

$$\mathbb{E}_X[X] \leqslant \mathcal{E}, \tag{2}$$

$$0 \leqslant X \leqslant A, \tag{3}$$

where $\mathcal{E}$ and A denote the allowed average power limit and allowed peak power limit, respectively. By using the "less than or equal to" constraint in Eq. (2), we avoid that the system is forced to operate at full power. The ratio between $\mathcal{E}$ and A is defined as

$$\varepsilon \triangleq \frac{\mathcal{E}}{A}, \quad 0 < \varepsilon \leqslant 1. \tag{4}$$

The capacity with average and peak optical power constraints is denoted as $C(A, \mathcal{E})$.

Under the constraints in Eqs. (3) and (2), this work analyzes the upper and lower bounds on the channel capacity for nonlinear receiver OWC systems.

III. Capacity Bound of the Nonlinear SISO System

A. Lower Bound for SISO System

The capacity, as the maximum mutual information between input and output signals over all input distributions, can be expressed as

$$\begin{aligned} C &= \max_{f_X(x)} I(X;R) = \max_{f_X(x)} [h(R) - h(R|X)] \\ &= \max_{f_X(x)} h(\phi(HX) + n) - h(n). \end{aligned} \tag{5}$$

where $h(X) = -\int_{-\infty}^{\infty} f_X(x) \ln f_X(x) \mathrm{d}x$, and $f_X(x)$ denotes the probability density function (PDF) of X. From Eq. (5), a lower bound can be derived as

$$C = \max_{f_X(x)} h(\phi(HX) + n) - h(n) \tag{6a}$$

$$\geqslant \frac{1}{2} \ln \left[e^{2h(\phi(HX))} + e^{2h(n)} \right] - h(n) \tag{6b}$$

$$= \frac{1}{2} \ln \left[1 + \frac{e^{2h(\phi(HX))}}{2\pi e \sigma^2} \right], \tag{6c}$$

where the inequality in Eq. (6b) follows from EPI.

Define new random variable $Y = \phi(HX)$. The PDF $f_Y(y)$ of Y can be obtained as follows. Solve the equation $y = \phi(Hx)$ under condition $H = h_{11}$ (where subscript "11" indicates SISO) and $Y = y$. Define x_i as the i-th real root of the equation $y = \phi(h_{11}x)$, i.e.,

$$y = \phi(h_{11}x_1) = \cdots = \phi(h_{11}x_i) = \cdots, y \in [0, \alpha], \tag{7}$$

$$x_1, \cdots, x_i, \cdots \in [0, A]. \tag{8}$$

We divide the nonlinear function into smaller intervals of x, where the nonlinear function within each interval of x is monotonous, as illustrated in Fig. 2. For values of y within each where $\phi(h_{11}x)$ is one-to-one, the inverse function can be defined as

$$x_1 = x_1(y), \cdots, x_i = x_i(y), \cdots. \tag{9}$$

The PDF of Y can be expressed as [33]

$$\begin{aligned} & f_Y(y) \\ &= \frac{f_X(x_1)}{|\phi'(h_{11}x_1)|}\bigg|_{x_1=x_1(y)} + \cdots + \frac{f_X(x_i)}{|\phi'(h_{11}x_i)|}\bigg|_{x_i=x_i(y)} + \cdots \\ &= \sum_{i=1}^{\psi(y)} \frac{f_X(x_i)}{|\phi'(h_{11}x_i)|}\bigg|_{x_i=x_i(y)} \end{aligned} \tag{10}$$

where $\phi'(h_{11}x)$ is the derivative of $\phi(h_{11}x)$ with respect to x; $p(x)|_{x=q(y)}$ denotes that $p(x)$ is first evaluated and then x is substituted with $q(x)$. If Eq. (7) has no real roots for given y and h_{11}, then $f_Y(y) = 0$. Define a function $\psi(y)$ to represent the number of real roots x_i for a given y.

Then, the differential entropy of Y, denoted as $h(y)$, is provided by Eq. (11).

Applying Jensen's inequality to convex function $\kappa(u) = u \ln u$ with $u>0$, we have

$$\kappa\left(\frac{1}{n}\sum_{i=1}^{n} u_i\right) \leqslant \frac{1}{n}\sum_{i=1}^{n} \kappa(u_i), \text{for all } u_1, u_2, \cdots, > 0. \tag{12}$$

Setting $n = \psi(y)$ and $u_i = \frac{\psi(y) f_X(x_i)}{|\phi'(h_{11}x_i)|}\Big|_{x_i=x_i(y)}$ in Eq. (12), Eq. (11) is lower bounded by Eq. (13).

Noting that $y = \phi(h_{11}x)$, the substitution is introduced to simplify the expression, and Jacobian determinant is calculated to eliminate the denominators in each term. Additionally, the logarithmic terms inside $\ln(\cdot)$ are decomposed into two parts to facilitate the application of EPI. As a result, Eq. (11) can

$$
\begin{aligned}
&h\left(\phi\left(h_{11}X\right)\right)=h\left(Y\right)=-\int_{0}^{\alpha}f_{Y}\left(y\right)\ln f_{Y}\left(y\right)\mathrm{d}y\\
&=-\int_{0}^{\alpha}\left[\frac{f_{X}(x_1)}{\left|\phi'\left(h_{11}x_1\right)\right|}\bigg|_{x_1=x_1(y)}+\cdots+\frac{f_{X}(x_i)}{\left|\phi'\left(h_{11}x_i\right)\right|}\bigg|_{x_i=x_i(y)}+\cdots\right]\ln\left[\frac{f_{X}(x_1)}{\left|\phi'\left(h_{11}x_1\right)\right|}\bigg|_{x_1=x_1(y)}+\cdots+\frac{f_{X}(x_i)}{\left|\phi'\left(h_{11}x_i\right)\right|}\bigg|_{x_i=x_i(y)}+\cdots\right]\mathrm{d}y\\
&=-\int_{0}^{\alpha}\left[\sum_{i=1}^{\psi(y)}\frac{f_{X}\left(x_i\right)}{\left|\phi'\left(h_{11}x_i\right)\right|}\bigg|_{x_i=x_i(y)}\right]\ln\left[\sum_{i=1}^{\psi(y)}\frac{f_{X}\left(x_i\right)}{\left|\phi'\left(h_{11}x_i\right)\right|}\bigg|_{x_i=x_i(y)}\right]\mathrm{d}y.
\end{aligned}
\tag{11}
$$

$$
\begin{aligned}
h\left(Y\right)&\geqslant-\int_{0}^{\alpha}\left[\frac{f_{X}\left(x_1\right)}{\left|\phi'\left(h_{11}x_1\right)\right|}\ln\frac{\psi\left(y\right)f_{X}\left(x_1\right)}{\left|\phi'\left(h_{11}x_1\right)\right|}\right]\bigg|_{x_1=x_1(y)}+\cdots+\left[\frac{f_{X}\left(x_i\right)}{\left|\phi'\left(h_{11}x_i\right)\right|}\ln\frac{\psi\left(y\right)f_{X}\left(x_i\right)}{\left|\phi'\left(h_{11}x_i\right)\right|}\right]\bigg|_{x_i=x_i(y)}+\cdots\mathrm{d}y\\
&=-\int_{0}^{\alpha}\sum_{i=1}^{\psi(y)}\left[\frac{f_{X}\left(x_i\right)}{\left|\phi'\left(h_{11}x_i\right)\right|}\ln\frac{\psi\left(y\right)f_{X}\left(x_i\right)}{\left|\phi'\left(h_{11}x_i\right)\right|}\right]\bigg|_{x_i=x_i(y)}\mathrm{d}y.
\end{aligned}
\tag{13}
$$

be simplified to

$$
h\left(Y\right)\geqslant-\int_{0}^{A}f_{X}\left(x\right)\left[\ln\psi\left(\phi\left(h_{11}x\right)\right)+\ln\frac{f_{X}\left(x\right)}{\left|\phi'\left(h_{11}x\right)\right|}\right]\mathrm{d}x. \tag{14}
$$

A tight lower bound is determined by the input distribution that maximizes the right-hand side of Eq. (14), subject to the average and peak optical power constraints. The related optimization problem is formulated as

$$
\max_{f_X(x)}-\int_{0}^{A}f_{X}\left(x\right)\left[\ln\psi\left(\phi\left(h_{11}x\right)\right)+\ln\frac{f_{X}\left(x\right)}{\left|\phi'\left(h_{11}x\right)\right|}\right]\mathrm{d}x \tag{15}
$$

$$
\text{s.t.}\qquad\int_{0}^{A}f_{X}\left(x\right)dx=1, \tag{16}
$$

$$
\int_{0}^{A}xf_{X}\left(x\right)dx\leqslant\mathcal{E}, \tag{17}
$$

$$
f_{X}\left(x\right)\geqslant0. \tag{18}
$$

According [34, Theorem 12.1.1], the optimal form of $f_X\left(x\right)$ is given by

$$
f_{X}\left(x\right)=\left|\phi'\left(h_{11}x\right)\right|e^{\lambda_1+\lambda_2x-1-\ln\psi(\phi(h_{11}x))}, \tag{19}
$$

where $\lambda_1>0$ and $\lambda_2>0$ are chosen to satisfy Eqs. (16) and (17).

Substituting Eq. (19) into Eq. (14), we have

$$
\begin{aligned}
h\left(Y\right)&\geqslant-\int_{0}^{A}f_{X}\left(x\right)\left(\lambda_1+\lambda_2x-1\right)dx &(20)\\
&=-\left(\lambda_1+1-\lambda_2\mathbb{E}_{X}\left[X\right]\right), &(21)
\end{aligned}
$$

where $\mathbb{E}_X\left[X\right]$ is the expectation of X. Let λ_1^* and λ_2^* denote the values of λ_1 and λ_2 that maximize Eq. (21). Then, the lower bound is given by

$$
C\left(A,\mathcal{E}\right)\geqslant\frac{1}{2}\ln\left[1+\frac{e^{2(-\lambda_1^*+1-\lambda_2^*\mathbb{E}_X[X])}}{2\pi e\sigma^2}\right]. \tag{22}
$$

B. Upper Bound for SISO System

An upper bound on the OWC channel capacity can be written as

$$
C\leqslant\max_{f_X(x)}\mathbb{E}_{X}\left[D\left(P_{R|X}\left(r\left|x\right.\right)\|V_{R}\left(r\right)\right)\right], \tag{23}
$$

$$
D\left(P_{R|X}\left(r\left|x\right.\right)\|V_{R}\left(r\right)\right)=\int P_{R|X}\left(r\left|x\right.\right)\ln\frac{P_{R|X}(r\left|x\right.)}{V_{R}\left(r\right)}\mathrm{d}r, \tag{24}
$$

where $V_R\left(r\right)$ is any choice of "test" density on the output signal space. To obtain a relatively tight upper bound close to the actual channel capacity, delicate consideration of $V_R\left(r\right)$ is required. We select $V_R\left(r\right)$ as Eq. (25) shown in Fig. 3.

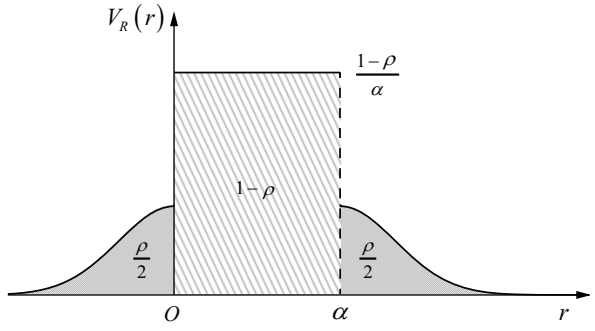

Fig. 3. Test density $V_R\left(r\right)$ for SISO OWC.

$$
V_{R}\left(r\right)=\begin{cases}\frac{\rho}{\sqrt{2\pi}\sigma}e^{-\frac{r^2}{2\sigma^2}} & r\leqslant0\\ \frac{1-\rho}{\alpha} & 0<r\leqslant\alpha\\ \frac{\rho}{\sqrt{2\pi}\sigma}e^{-\frac{(r-\alpha)^2}{2\sigma^2}} & r>\alpha\end{cases}, \tag{25}
$$

where $\rho\in[0,1]$ is the parameter to be optimized. $V_R\left(r\right)$ is composed of two scaled distributions: a uniform distribution over the interval $(0,\alpha]$ and truncated Gaussian distributions over the intervals $(-\infty,0]$ and (α,∞).

For the nonlinear receiver system described by Eq. (1), conditional PDF $P_{R|X}\left(r\left|x\right.\right)$ can be expressed as

$$P_{R|X}\left(r\left|x\right.\right)=\frac{1}{\sqrt{2\pi}\sigma}e^{-\frac{[r-\phi(h_{11}x)]^2}{2\sigma^2}}. \tag{26}$$

Substituting Eqs. (26) and (25) into the relative entropy $D\left(P_{R|X}\left(r\left|x\right.\right)\left\|V_R\left(r\right)\right.\right)$, we have the following result.

Theorem 1 *Based on Eqs. (25) and (26), Eq. (24) is upper bounded by*

$$D\left(P_{R|X}\left(r\left|x\right.\right)\left\|V_R\left(r\right)\right.\right)\leqslant\ln\frac{1}{\rho}+\vartheta\left(y\right)\ln\frac{\alpha\rho}{\sqrt{2\pi e}\sigma\left(1-\rho\right)},$$

$$\vartheta\left(y\right)=Q\left(-\frac{y}{\sigma}\right)-Q\left(\frac{\alpha-y}{\sigma}\right), \tag{27}$$

where $y=\phi\left(h_{11}x\right)$*, and*

$$Q\left(p\right)=\int_p^{\infty}\frac{1}{\sqrt{2\pi}}e^{-\frac{x^2}{2}}dx. \tag{28}$$

Proof: Please refer to Appendix A. ■

The upper bound in Eq. (23) can be rewritten as

$$C\leqslant\max_{f_X(x)}\mathbb{E}_X\left[\ln\frac{1}{\rho}+\vartheta\left(\phi\left(h_{11}x\right)\right)\ln\frac{\alpha\rho}{\sqrt{2\pi e}\sigma\left(1-\rho\right)}\right]. \tag{29}$$

The next step is to solve the optimization problem on the right-hand side of Eq. (29), subject to the non-negativity, average optical power, and peak optical power constraints in Eqs. (15)-(17).

Letting $y=\phi\left(h_{11}x\right)$, we have

$$\mathbb{E}_X\left[\ln\frac{1}{\rho}+\vartheta\left(\phi\left(h_{11}x\right)\right)\ln\frac{\alpha\rho}{\sqrt{2\pi e}\sigma\left(1-\rho\right)}\right]$$
$$=\mathbb{E}_Y\left[\ln\frac{1}{\rho}+\vartheta\left(y\right)\ln\frac{\alpha\rho}{\sqrt{2\pi e}\sigma\left(1-\rho\right)}\right]. \tag{30}$$

The optimization problem in the right-hand side of Eq. (29) is formulated as

$$\max_{f_Y(y)}\mathbb{E}_Y\left[\ln\frac{1}{\rho}+\vartheta\left(y\right)\ln\frac{\alpha\rho}{\sqrt{2\pi e}\sigma\left(1-\rho\right)}\right] \tag{31}$$

$$\text{s.t.}\quad\int_0^{\alpha}f_Y\left(y\right)\mathrm{d}y=1, \tag{32}$$

$$\int_0^{\alpha}yf_Y\left(y\right)\mathrm{d}y\leqslant\max_{f_X(x)}\int_0^{A}\phi\left(h_{11}x\right)f_X\left(x\right)\mathrm{d}x, \tag{33}$$

$$f\left(y\right)\geqslant 0. \tag{34}$$

Let $E_Y^*=\max\limits_{f_X(x)}\int_0^{A}\phi\left(h_{11}x\right)f_X\left(x\right)\mathrm{d}x$ in Eq. (33). For notational simplicity, define the function $T\left(\rho,y\right)$ as

$$T\left(\rho,y\right)=\ln\frac{1}{\rho}+\vartheta\left(y\right)\ln\frac{\alpha\rho}{\sqrt{2\pi e}\sigma\left(1-\rho\right)}. \tag{35}$$

When $y\in[0,\alpha]$, the second derivative of $\vartheta\left(y\right)$ can be expressed as

$$\frac{\partial^2\vartheta}{\partial y^2}=\frac{1}{\sqrt{2\pi}\sigma^3}\left[e^{-\frac{(y-\alpha)^2}{2\sigma^2}}\left(y-\alpha\right)-e^{-\frac{y^2}{2\sigma^2}}y\right]<0. \tag{36}$$

Note that for all $y\in[0,\alpha]$, the second derivative of $\vartheta\left(y\right)$ is non-positive, and thus $\vartheta\left(y\right)$ is concave. Then, we have

$$\int_0^{\alpha}f_Y\left(y\right)\vartheta\left(y\right)\mathrm{d}y\leqslant\vartheta\left(\int_0^{\alpha}f_Y\left(y\right)y\mathrm{d}y\right)\leqslant\max\vartheta\left(y\right). \tag{37}$$

From the Eqs. (35) and (37), it is observed that when $\ln\frac{\alpha\rho}{\sqrt{2\pi e}\sigma(1-\rho)}\geqslant 0$, the second term of $T\left(\rho,y\right)$ is concave with respect to y, and we have

$$\max_{f_Y(y)}\mathbb{E}_Y\left[T\left(\rho,y\right)\right]\leqslant T\left(\rho,\zeta^*\right), \tag{38}$$

$$\zeta^*=\min\left\{E_Y^*,\alpha/2\right\}. \tag{39}$$

When $\ln\frac{\alpha\rho}{\sqrt{2\pi e}\sigma(1-\rho)}<0$, the second term of $T\left(\rho,y\right)$ is convex with respect to y, and we have

$$\max_{f_Y(y)}\mathbb{E}_Y\left[T\left(\rho,y\right)\right]\leqslant T\left(\rho,\alpha\right). \tag{40}$$

The next step is to minimize the right-hand sides of Eqs. (38) and (40) through optimizing ρ, to derive the upper bound on the SISO system. Note that for $\rho\in[0,1]$, the second derivative of $T\left(\rho,y\right)$ is non-positive, and thus $T\left(\rho,y\right)$ is convex with respect to ρ. The minimum value of $T\left(\rho,y\right)$ occurs when $\rho=1-\vartheta\left(y\right)$. Note that $1-\vartheta\left(\alpha\right)\geqslant 1-\vartheta\left(\zeta^*\right)$, we have the following result.

Case 1 *If*

$$1-\vartheta\left(\zeta^*\right)>\frac{\sqrt{2\pi e}\sigma}{\alpha+\sqrt{2\pi e}\sigma}, \tag{41}$$

then

$$C\left(A,\mathcal{E}\right)\leqslant T\left(1-\vartheta\left(\zeta^*\right),\zeta^*\right). \tag{42}$$

Case 2 *If*

$$1-\vartheta\left(\alpha\right)<\frac{\sqrt{2\pi e}\sigma}{\alpha+\sqrt{2\pi e}\sigma}, \tag{43}$$

then

$$C\left(A,\mathcal{E}\right)\leqslant T\left(1-\vartheta\left(\alpha\right),\alpha\right). \tag{44}$$

Case 3 *If*

$$1-\vartheta\left(\zeta^*\right)<\frac{\sqrt{2\pi e}\sigma}{\alpha+\sqrt{2\pi e}\sigma}<1-\vartheta\left(\alpha\right), \tag{45}$$

then

$$C\left(A,\mathcal{E}\right)\leqslant\min\left\{T\left(1-\vartheta\left(\zeta^*\right),\zeta^*\right),T\left(1-\vartheta\left(\alpha\right),\alpha\right)\right\}. \tag{46}$$

Case 4 *If*

$$1-\vartheta\left(\zeta^*\right)=\frac{\sqrt{2\pi e}\sigma}{\alpha+\sqrt{2\pi e}\sigma}\ \ or\ \ 1-\vartheta\left(\alpha\right)=\frac{\sqrt{2\pi e}\sigma}{\alpha+\sqrt{2\pi e}\sigma}, \tag{47}$$

then

$$C\left(A,\mathcal{E}\right)\leqslant\ln\left(1+\frac{\alpha}{\sqrt{2\pi e}\sigma}\right). \tag{48}$$

IV. Capacity Bound of the Nonlinear MIMO System

A. Generalized Lower Bound to $M \times M$ MIMO System

According to Eq. (1), the transmission model of an $M \times M$ MIMO system can be written as

$$\boldsymbol{R} = \boldsymbol{\Phi}\left(\boldsymbol{H}\boldsymbol{X}\right) + \boldsymbol{N}, \tag{49}$$

where $\boldsymbol{X} = [X_1, X_2, \cdots, X_M]$ and $\boldsymbol{R} = [R_1, R_2, \cdots, R_M]$ denote the transmitted and received vectors, respectively; $\boldsymbol{H} \in \mathbb{R}_+^{M\times M}$ denotes the channel matrix with each element being the link gain of the corresponding transmission path; $\boldsymbol{N} \sim \mathcal{N}(\boldsymbol{0}, \sigma^2\mathbf{I})$ denotes the noise vector. The MIMO channel capacity is lower bounded by

$$C \geqslant \frac{M}{2}\ln\left[1 + \frac{e^{\frac{2}{M}\ h(\boldsymbol{\Phi}(\boldsymbol{H}\boldsymbol{X}))}}{2\pi e\sigma^2}\right]. \tag{50}$$

In commercial communication systems, the receiver often consists of identical units. Thus, we assume that all receivers exhibit the same non-linear characteristics. Considering an $M \times M$ MIMO system, assume that each receiver nonlinear characteristics take the form as described in Section.II. Define the vectors $\boldsymbol{Y} = [Y_1, Y_2, \cdots, Y_M]$ and $\boldsymbol{Z} = [Z_1, Z_2, \cdots, Z_M]$ such that $\boldsymbol{Y} = \boldsymbol{\Phi}\left(\boldsymbol{H}\boldsymbol{X}\right)$ and $\boldsymbol{Z} = \boldsymbol{H}\boldsymbol{X}$. Given $\boldsymbol{H} = \boldsymbol{h}$ and $\boldsymbol{Y} = \boldsymbol{y}$, we have

$$\boldsymbol{y} = \boldsymbol{\Phi}\left(\boldsymbol{z}\right) = \boldsymbol{\Phi}\left(\boldsymbol{h}\boldsymbol{x}\right), \tag{51}$$

where $y_i \in [0, \alpha_i]$, $i = 1, 2, \cdots, M$.

For a given $\boldsymbol{y}$ and $\boldsymbol{h}$, Eq. (51) may have multiple real solutions. These are denoted as $\boldsymbol{x}_1$, $\boldsymbol{x}_2$, $\cdots$, $\boldsymbol{x}_i$, $\cdots$. Specifically, the i-th real solution can be described as

$$\boldsymbol{\Phi}\left(\boldsymbol{z}\right)_{\boldsymbol{x}=\boldsymbol{x}_i} = \boldsymbol{y}, \tag{52}$$

For M-dimensional case, $\psi\left(\boldsymbol{y}\right)$ is defined as the number of real solutions that satisfy Eq. (51) for a given $\boldsymbol{y}$ and $\boldsymbol{h}$.

Based on the Jacobian transformation, the joint PDF of Y_1, Y_2, $\cdots$, Y_M, $f_{\boldsymbol{Y}}\left(\boldsymbol{y}\right)$, can be expressed as

$$f_{\boldsymbol{Y}}\left(\boldsymbol{y}\right) = \sum_{i=1}^{\psi(\boldsymbol{y})} \frac{f_{\boldsymbol{X}}\left(\boldsymbol{x}_i\right)}{\left|\boldsymbol{J}\left(\boldsymbol{x}_i\right)\right|}\Bigg|_{\boldsymbol{x}_i=\boldsymbol{x}_i(\boldsymbol{y})}, \tag{53}$$

where $\boldsymbol{J}(\boldsymbol{x}_i)$ represents the Jacobian determinant of $\boldsymbol{x}_i$. If Eq. (51) has no real solutions for given $\boldsymbol{y}$ and $\boldsymbol{h}$, then the joint PDF $f_{\boldsymbol{Y}}\left(\boldsymbol{y}\right) = 0$.

Based on Eq. (53), the differential entropy $h\left(\boldsymbol{Y}\right)$ of $\boldsymbol{Y}$ for a given $\boldsymbol{h}$ is expressed as Eq. (54), where $\boldsymbol{\alpha} = [\alpha_0, \alpha_1, \cdots, \alpha_M]$.

Letting $u_i = \frac{\psi(\boldsymbol{y}) f_{\boldsymbol{X}}(\boldsymbol{x}_i)}{|\boldsymbol{J}(\boldsymbol{x}_i)|}\Big|_{\boldsymbol{x}_i=\boldsymbol{x}_i(\boldsymbol{y})}$ in Eq. (12), a lower bound for Eq. (54) is given by

$$h\left(\boldsymbol{Y}\right) \geqslant -\int_{\boldsymbol{0}}^{\boldsymbol{\alpha}} \sum_{i=1}^{\psi(\boldsymbol{y})} \left[\frac{f_{\boldsymbol{X}}\left(\boldsymbol{x}_i\right)}{\left|\boldsymbol{J}\left(\boldsymbol{x}_i\right)\right|} \ln \frac{\psi\left(\boldsymbol{y}\right) f_{\boldsymbol{X}}\left(\boldsymbol{x}_i\right)}{\left|\boldsymbol{J}\left(\boldsymbol{x}_i\right)\right|}\right]\Bigg|_{\boldsymbol{x}_i=\boldsymbol{x}_i(\boldsymbol{y})} \mathrm{d}\boldsymbol{y}. \tag{55}$$

By employing the substitution method $\boldsymbol{\Phi}\left(\boldsymbol{h}\boldsymbol{x}\right) = \boldsymbol{y}$, Eq. (55) can be simplified as Eq. (56).

$$h\left(\boldsymbol{Y}\right) \geqslant -\int_{\boldsymbol{0}}^{\boldsymbol{A}} f_{\boldsymbol{X}}\left(\boldsymbol{x}\right)\left[\ln \psi\left(\boldsymbol{y}\right) + \ln \frac{f_{\boldsymbol{X}}\left(\boldsymbol{x}\right)}{\left|\boldsymbol{J}\left(\boldsymbol{x}\right)\right|}\right]\mathrm{d}\boldsymbol{x}. \tag{56}$$

Assuming that each transmitter is discretely placed, each transmitter has its own independent power supply and driving circuitry to prevent additional transmitter-side nonlinearities, positioned independently to reduce subchannel correlation and ensuring that the channel matrix maintains full rank. Each LED must comply with the non-negative constraint, the average power constraint, and the peak power constraint, which are given as follows,

$$\int_{\boldsymbol{0}}^{\boldsymbol{A}} f_{\boldsymbol{X}}\left(\boldsymbol{x}\right)\mathrm{d}\boldsymbol{x} = 1, \tag{57}$$

$$\int_{\boldsymbol{0}}^{\boldsymbol{A}} x_i f_{\boldsymbol{X}}\left(\boldsymbol{x}\right)\mathrm{d}\boldsymbol{x} \leqslant \mathcal{E}, i = 1, 2, \cdots, M, \tag{58}$$

$$f_{\boldsymbol{X}}\left(\boldsymbol{x}\right) \geqslant 0. \tag{59}$$

Since Eq. (50) holds for all $f_{\boldsymbol{X}}\left(\boldsymbol{x}\right)$ that satisfy Eqs. (57)-(59), a tight lower bound can be obtained by selecting an appropriate $f_{\boldsymbol{X}}\left(\boldsymbol{x}\right)$ that maximizes the right-hand side of Eq. (56) while meeting the aforementioned constraints. Formulating it as a standard optimization problem, similar to the SISO system, the optimal distribution $f_{\boldsymbol{X}}\left(\boldsymbol{x}\right)$ can be expressed as

$$f_{\boldsymbol{X}}\left(\boldsymbol{x}\right) = \left|\boldsymbol{J}\left(\boldsymbol{x}\right)\right| e^{\lambda_1 + \sum\limits_{i=1}^{M} \lambda_{i+1} x_i - 1 - \psi(\boldsymbol{y})}. \tag{60}$$

Thus,

$$h\left(\boldsymbol{Y}\right) \geqslant -\lambda_1 + 1 - \sum_{i=1}^{M} \lambda_{i+1}\mathbb{E}_{\boldsymbol{X}}\left[X_i\right], \tag{61}$$

where

$$\mathbb{E}_{\boldsymbol{X}}\left[X_i\right] = \int_{\boldsymbol{0}}^{\boldsymbol{A}} x_i f_{\boldsymbol{X}}\left(\boldsymbol{x}\right)\mathrm{d}\boldsymbol{x}. \tag{62}$$

Let λ_1^*, λ_2^*, $\cdots$, λ_{i+1}^* denote the values of λ_1, λ_2, $\cdots$, λ_{i+1} that maximize $-\lambda_1 + 1 - \sum\limits_{i=1}^{M} \lambda_{i+1}\mathbb{E}_{\boldsymbol{X}}\left[X_i\right]$. Therefore, the lower bound on the $M \times M$ MIMO system is given by

$$C\left(A, \mathcal{E}\right) \geqslant \frac{M}{2}\ln\left[1 + \frac{e^{\frac{2}{M}\left(-\lambda_1^* + 1 - \sum\limits_{i=1}^{M} \lambda_{i+1}^* \mathbb{E}_{\boldsymbol{X}}[X_i]\right)}}{2\pi e\sigma^2}\right]. \tag{63}$$

B. Generalized Upper Bound to $M \times M$ MIMO System

For the transmit vector $\boldsymbol{X} = [X_1, \cdots, X_M]$ and the receive vector $\boldsymbol{R} = [R_1, \cdots, R_M]$, when $\boldsymbol{h}$ is known, the conditional PDF $P_{\boldsymbol{R}|\boldsymbol{X}}\left(\boldsymbol{r}|\boldsymbol{x}\right)$ is given by

$$P_{\boldsymbol{R}|\boldsymbol{X}}\left(\boldsymbol{r}\,|\boldsymbol{x}\right) = \frac{1}{\left(2\pi\sigma^2\right)^{\frac{M}{2}}} e^{-\frac{\|\boldsymbol{r} - \boldsymbol{\Phi}(\boldsymbol{h}\boldsymbol{x})\|^2}{2\sigma^2}}. \tag{64}$$

Referring to Eq. (23), the upper bound on the $M \times M$ MIMO system is given by

$$C \leqslant \max_{f_{\boldsymbol{X}}(\boldsymbol{x})} \mathbb{E}_{\boldsymbol{X}}\left[D\left(P_{\boldsymbol{R}|\boldsymbol{X}}\left(\boldsymbol{r}\,|\boldsymbol{x}\right)\|V_{\boldsymbol{R}}\left(\boldsymbol{r}\right)\right)\right]. \tag{65}$$

$$D\left(P_{\boldsymbol{R}|\boldsymbol{X}}\left(\boldsymbol{r}\,|\boldsymbol{x}\right)\|V_{\boldsymbol{R}}(\boldsymbol{r})\right) = \int P_{\boldsymbol{R}|\boldsymbol{X}}\left(\boldsymbol{r}\,|\boldsymbol{x}\right)\ln\frac{P_{\boldsymbol{R}|\boldsymbol{X}}\left(\boldsymbol{r}\,|\boldsymbol{x}\right)}{V_{\boldsymbol{R}}(\boldsymbol{r})}\mathrm{d}\boldsymbol{r}. \tag{66}$$

We define the index set $S = \{1, 2, 3, ..., M\}$ and the sub-index sets S_1, S_2, $\cdots$, S_M, where

$$S_i = \left\{(s_1, s_2, \cdots, s_i)|\, s_1 < \cdots s_i, s_1, \cdots, s_i \in S\right\}, \tag{67}$$

$$h\left(\boldsymbol{Y}\right)=-\int_{\mathbf{0}}^{\boldsymbol{\alpha}}\left(\sum_{i=1}^{\psi(\boldsymbol{y})}\frac{f_{\boldsymbol{X}}\left(\boldsymbol{x}_i\right)}{\left|\boldsymbol{J}\left(\boldsymbol{x}_i\right)\right|}\Big|_{\boldsymbol{x}_i=\boldsymbol{x}_i(\boldsymbol{y})}\right)\ln\left(\sum_{i=1}^{\psi(\boldsymbol{y})}\frac{f_{\boldsymbol{X}}\left(\boldsymbol{x}_i\right)}{\left|\boldsymbol{J}\left(\boldsymbol{x}_i\right)\right|}\Big|_{\boldsymbol{x}_i=\boldsymbol{x}_i(\boldsymbol{y})}\right)\mathrm{d}\boldsymbol{y}. \tag{54}$$

where S_i has a total of C_M^i elements. We define $S_i\left(j\right)$ to be the jth element in the set S_i, $\widehat{S_i\left(j\right)}$ to be the complement of $S_i\left(j\right)$ with respect to S, that is, $\widehat{S_i\left(j\right)}$ contains all the elements that are in S but not in $S_i\left(j\right)$, $S_i(j,k)$ to be the kth element in $S_i\left(j\right)$ and $\boldsymbol{r}_{S_n(j)}=\left(r_{S_n(j,1)},r_{S_n(j,2)},\cdots r_{S_n(j,n)}\right)$, $\boldsymbol{\alpha}_{S_n(j)}=\left(\alpha_{S_n(j,1)},\alpha_{S_n(j,2)},\cdots\alpha_{S_n(j,n)}\right)$, respectively. Given the M-dimensional amplitude constraint as defined in Eq. (3), we have selected a test density $V_{\boldsymbol{R}}(\boldsymbol{r})$ as Eq. (68).

In Eq. (68) ρ_0, ρ_1, $\cdots$, $\rho_{M-1}\in[0,1]$ are to be optimized. Similarly, the test density is uniform in the closed area $\left\{\boldsymbol{r}_S\middle|\,\boldsymbol{r}_S\in[0,\boldsymbol{\alpha}_S]\right\}$ and is a "split and scaled" Gaussian distribution in area $\left\{\boldsymbol{r}_{S_n(j)}\middle|\,\boldsymbol{r}_{S_n(j)}\in\left[0,\boldsymbol{\alpha}_{S_n(j)}\right]\right\}$. Assume that $M=2$, the test density in R_1OR_2 plane is shown in Fig. 4.

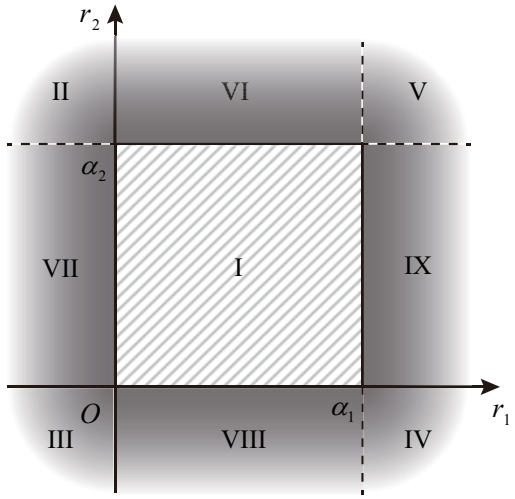

Fig. 4. Test density $V_{\boldsymbol{R}}\left(\boldsymbol{r}\right)$ for 2×2 MIMO OWC.

Substituting Eqs. (64) and (68) into Eq. (66), we have the following result.

Theorem 2 *For Eqs. (64) and (68), Eq. (66) is upper bounded by*

$$\begin{aligned}&D\left(P_{\boldsymbol{R}|\boldsymbol{X}}\left(\boldsymbol{r}\left|\boldsymbol{x}\right.\right)\|V_{\boldsymbol{R}}(\boldsymbol{r})\right)\\&\quad\leqslant T\left(\rho_0,\cdots,\rho_M,\phi\left(\mathbb{h}_1\boldsymbol{x}\right),\cdots,\phi\left(\mathbb{h}_M\boldsymbol{x}\right)\right),\end{aligned}\tag{69}$$

where $\mathbb{h}_i=[h_{i1},h_{i2},\cdots,h_{iM}]$ is the ith row of channel matrix $\boldsymbol{h}$, and $T\left(\rho_0,\cdots,\rho_M,\phi\left(\mathbb{h}_1\boldsymbol{x}\right),\cdots,\phi\left(\mathbb{h}_M\boldsymbol{x}\right)\right)$ is defined by Eq. (70).

Proof: Please refer to Appendix B. ■

After scaling, the problem of finding the upper bound of channel capacity equivalent to maximizing the right-hand side of Eq. (69) through the selection of $f_{\boldsymbol{X}}\left(\boldsymbol{x}\right)$, under the constraints similar to Eqs. (57)-(59).

Formulate a new optimization problem as an upper bound to the original optimization problem. The new optimization problem is defined as

$$\max_{f_{\boldsymbol{Y}}(\boldsymbol{y})}\mathbb{E}_{\boldsymbol{Y}}\left[T\left(\rho_0,\cdots,\rho_M,\phi\left(\mathbb{h}_1\boldsymbol{x}\right),\cdots,\phi\left(\mathbb{h}_M\boldsymbol{x}\right)\right)\right]\tag{71}$$

$$\text{s.t.}\quad\int_{\mathbf{0}}^{\boldsymbol{\alpha}}f_{\boldsymbol{Y}}\left(\boldsymbol{y}\right)\mathrm{d}\boldsymbol{y}=1,\tag{72}$$

$$\int_{\mathbf{0}}^{\boldsymbol{\alpha}}y_i f_{\boldsymbol{Y}}\left(\boldsymbol{y}\right)\mathrm{d}\boldsymbol{y}\leqslant E_{Y_i}^{*},i=1,2,\cdots,M,\tag{73}$$

$$f_{\boldsymbol{Y}}\left(\boldsymbol{y}\right)\geqslant 0.\tag{74}$$

The assertion that the optimal value of the new optimization problem is an upper bound to the optimal value of the original problem has been discussed in Section III-B and is omitted here for brevity.

Since $\vartheta\left(\alpha,y\right)$ is a concave function with respect to y, we have

$$\mathbb{E}_{\boldsymbol{Y}}\left[Q(\alpha_i,y_i)\right]\leqslant Q\left(\alpha_i,\mathbb{E}_{\boldsymbol{Y}}\left[Y_i\right]\right)\leqslant\max Q\left(\alpha_i,y_i\right).\tag{75}$$

Minimizing the upper bounds through optimizing ρ_0, ρ_1, $\cdots$, ρ_M can yield relatively tight upper bounds. The computation of these function maximums and minimums can be conducted through numerical simulations on a computer.

V. Simulation Results and Discussion

This section conduct a numerical analysis of the upper and lower bounds of channel capacity for OWC with nonlinear receiver. Given the diversity in the performance forms of the "input-output" nonlinear functions of receivers, this section outlines several common nonlinear functions and assumes a piecewise form of a nonlinear function. Based on the simulation results, this section discusses the relationship among the upper and lower bounds and the forms of nonlinear functions, considering factors such as average power constraints, peak power constraints, and link gain. We consider four kinds of nonlinear receiver functions. The first is the nonlinear hard clipping function, typically caused by the non-ideal characteristics of ADCs and APDs, given by

$$\phi\left(z\right)=\begin{cases}z & 0\leqslant z<\beta\\ \beta & \beta\leqslant z\end{cases}.\tag{76}$$

At this case, $\psi(\beta)=\infty$.

The second is the nonlinear soft clipping function, usually due to the non-ideal characteristics of power amplifiers, is given by

$$\phi\left(z\right)=\frac{\beta z}{\left(1+z^{2k}\right)^{\frac{1}{2k}}},\tag{77}$$

where β represents the clipping threshold, and k is a model parameter.

Another nonlinear receiver function is described by a polynomial approximation model, typically due to the non-ideal

$$V_{\boldsymbol{R}}(\boldsymbol{r}) = \begin{cases} \dfrac{1-\sum\limits_{k=0}^{M-1}\rho_k}{\prod\limits_{j=1}^{M}\alpha_j} & \left\{\boldsymbol{r}_S \middle| \boldsymbol{r}_S \in [0, \boldsymbol{\alpha}_S]\right\} \\ \dfrac{\rho_n}{(2\pi\sigma^2)^{\frac{M-n}{2}} \prod\limits_{k=1}^{n}\alpha_{S_n(j,k)} C_M^n} e^{-\frac{\left\|\left|\boldsymbol{r}_{S_n(j)} - \boldsymbol{\alpha}_{S_n(j)}/2\right| - \boldsymbol{\alpha}_{S_n(j)}/2\right\|^2}{2\sigma^2}} & \left\{\boldsymbol{r}_{S_n(j)} \middle| \boldsymbol{r}_{S_n(j)} \in \left[0, \boldsymbol{\alpha}_{S_n(j)}\right]\right\} \end{cases}. \tag{68}$$

$$T\left(\rho_0, \cdots, \rho_M, \phi\left(\mathbb{h}_1 \boldsymbol{x}\right), \cdots, \phi\left(\mathbb{h}_M \boldsymbol{x}\right)\right) = -\frac{1}{2}\ln\left(2\pi e\right)^M |\boldsymbol{K}| + \prod_{i=1}^{M}\vartheta\left(\alpha_i, y_i\right)\ln\frac{\prod\limits_{j=1}^{M}\alpha_j}{1-\sum\limits_{k=0}^{M-1}\rho_k}$$
$$+\sum_{m=0}^{M-1}\sum_{n=1}^{C_M^m}\left\{\prod_{p\in S_m(n)}\vartheta\left(\alpha_p, y_p\right)\prod_{q\in\widehat{S_m(n)}}\left[1-\vartheta\left(\alpha_q, y_q\right)\right]\ln\frac{\left(2\pi e\sigma^2\right)^{\frac{M-m}{2}}\prod\limits_{l\in S_m(n)}\alpha_l C_M^m}{\rho_m}\right\}.$$
$$\vartheta\left(\alpha, y\right) = Q\left(-\frac{y}{\sigma}\right) - Q\left(\frac{\alpha - y}{\sigma}\right). \tag{70}$$

characteristics of LNAs, given by

$$\phi\left(z\right) = \beta_1 z + \beta_2 z^2 + \beta_3 z^3 + \beta_4 z^4 + \cdots, \tag{78}$$

where β_i denotes the gain at the ith order ($i = 1, 2, 3, \cdots$), with β_1 known as the linear gain.

The last nonlinear receiver function considers the complex form of the nonlinear function and opts for a piecewise approximation, given by

$$\phi\left(z\right) = \begin{cases} -\frac{\gamma}{\beta^2}z^2 + \frac{2\gamma}{\beta}z & 0 \leqslant z < \beta \\ \gamma e^{-z+\beta} & \beta \leqslant z \end{cases}. \tag{79}$$

By employing polynomial and piecewise approximations, we ensure that our model can capture a wide variety of nonlinear behaviors in practical systems. Although these two types of functions may not encompass all possible nonlinearities, they offer a high degree of generality and flexibility. This approach allows us to demonstrate the robustness and broad applicability of our analysis, which can be adapted to many real-world communication scenarios.

A. SISO System Simulation Results

Figure 5 shows the relationship between the upper and lower bounds of the channel capacity of a SISO OWC system with linear receiver ($\phi(z) = z$) and the peak power constraint A under different noise intensities ($h_{11} = 0.9$, $\varepsilon = 0.9$). If the receiver "input-output" function is ideally linear, then as the peak power constraint is relaxed, the upper and lower bounds of the channel capacity increase linearly with $\log_{10} A$, and the gap between the upper and lower bounds also decreases.

Figure 6 shows the relationship between the upper and lower bounds of the channel capacity for a SISO OWC system and the peak power constraint A ($h_{11} = 0.9$, $\varepsilon = 0.9$).

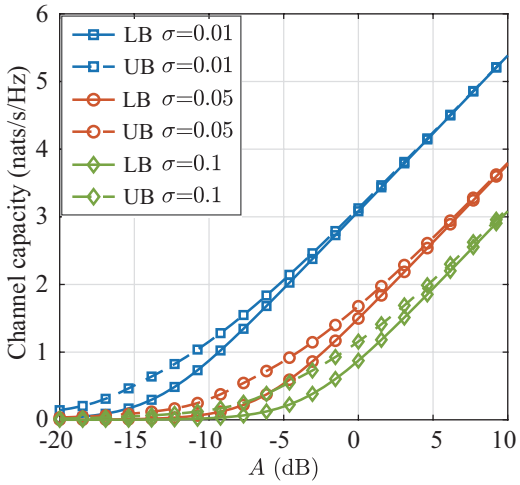

Fig. 5. Upper and lower bounds with respect to A for SISO OWC system with linear receiver ($h_{11} = 0.9$, $\varepsilon = 0.9$).

The results indicate that the form of the receiver nonlinear function significantly impacts the trend of channel capacity. In Figs. 6(a), (b), and (d), as the allowable peak power increases, the upper and lower bounds initially increase and then becomes stable, which contrasts with the increases seen in Fig. 5 as A increases for a linear receiver system. Additionally, increasing noise intensity degrades channel capacity and system performance, but the turning points and trends of the channel capacity bounds relative to A remain unchanged. This suggests that the recommended peak power constraints for the transmitted signal have consistency under different noise conditions for a given nonlinear receiver system. This conclusion is particularly important for outdoor OWC, where the granular noise from APDs increases with the intensity of background radiation. Moreover, the derivation of the upper

This article has been accepted for publication in IEEE Transactions on Wireless Communications. This is the author's version which has not been fully edited and content may change prior to final publication. Citation information: DOI 10.1109/TWC.2025.3559879

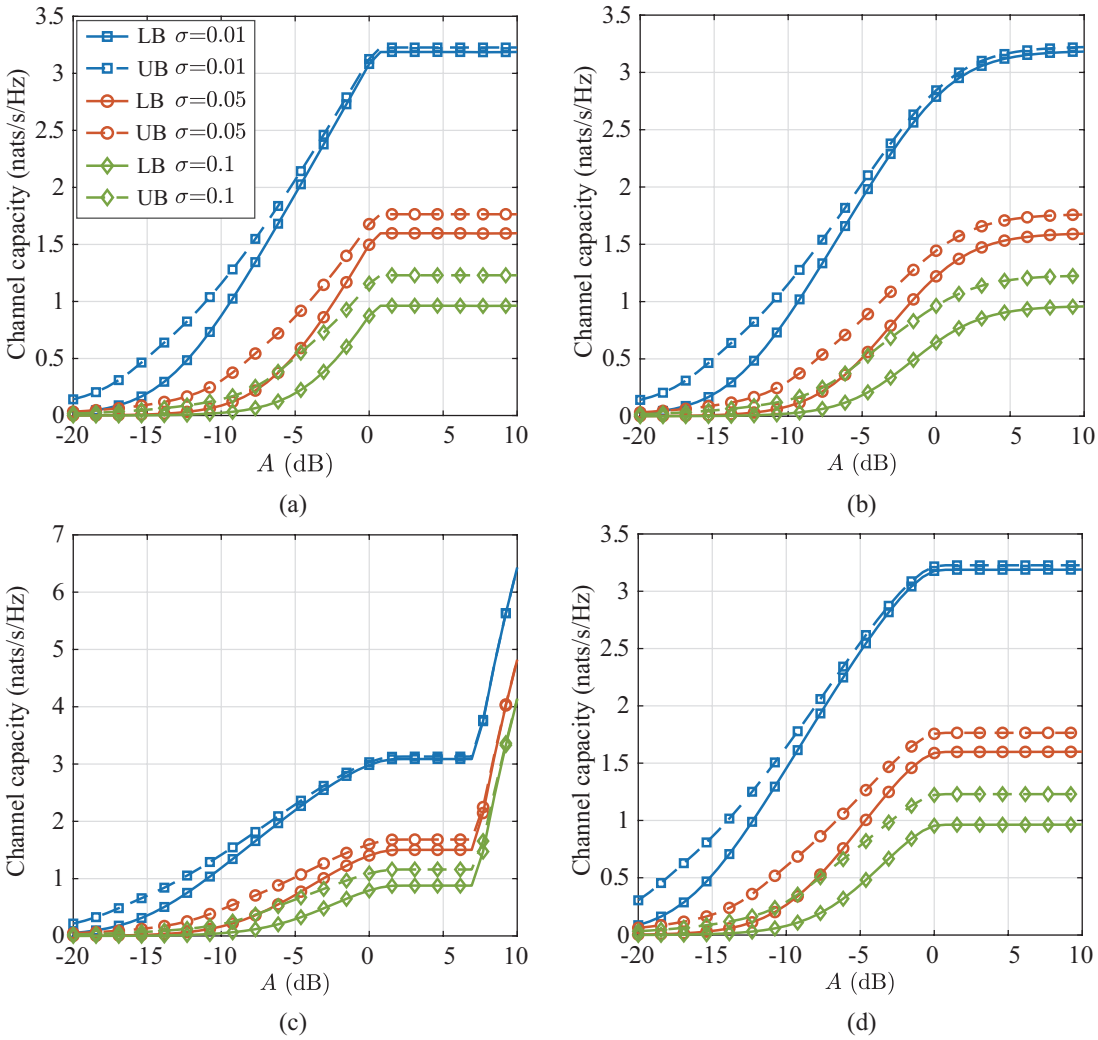

Fig. 6. Upper and lower bounds with respect to A for SISO OWC system with nonlinear receiver ($h_{11} = 0.9$, $\varepsilon = 0.9$). (a) Hard clipping ($\beta = 1$). (b) Soft clipping ($\beta = 1$, $k = 1$). (c) Polynomial approximation ($\beta_1 = 1.5$, $\beta_2 = -0.75$, $\beta_3 = 0.1$). (d) Piecewise approximation ($\gamma = 1$, $\beta = 1$).

and lower bounds of the channel capacity can guide the design of encoding strategies and power control schemes under different noise levels. Moreover, as the noise intensity increases, the gap between the upper and lower bounds of channel capacity also becomes larger since the entropy of noise increases with noise intensity. Moreover, the difference between the left and right terms in the Eq. (6) increases, thus widening the gap between the lower bound of the channel capacity and the actual channel capacity.

Figure 7 shows the gap between the upper and lower bounds of the channel capacity of a SISO nonlinear receiver system under different nonlinear receiver functions in relation to ε ($h_{11} = 0.9$, $A = 3$, $\sigma = 0.01$). The results show that as ε decreases, the gap between the upper and lower bounds of channel capacity also widens. This is due to the form of the $V_R(r)$ function, assuming the received signal distribution as a combination of a uniform distribution and two symmetrical single-sided truncated Gaussian distributions. This form implicitly suggests that the impact of the peak power constraint is greater compared to the average power constraint. When ε is greater than 0.3, the gap between the upper and lower

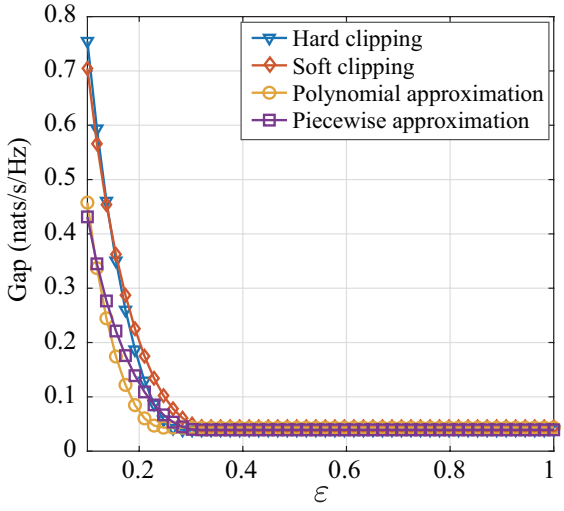

Fig. 7. The gap between the upper and lower bounds for SISO OWC system with respect to ε ($h_{11} = 0.9$, $A = 3$, $\sigma = 0.01$).

bounds of channel capacity converges to a smaller value. This indicates that the proposed channel capacity analysis method performs better under weaker average power constraints.

Figure 8 illustrates the relationship between the upper and lower bounds of the channel capacity of a SISO nonlinear receiver system and the link gain h_{11} under different nonlinear functions. The results indicate that the changes in channel capacity with increasing h_{11} are closely linked to the form of the nonlinear function used. For the four nonlinear functions simulated, at lower levels of h_{11}, increasing h_{11} effectively enhances the channel capacity. However, as h_{11} continues to rise, the changes in channel capacity reach a peak and then stabilize. This suggests that if the receiver "input-output" function is nonlinear, reducing the distance between the transmitter and receiver, or using lenses to increase the link gain between the transmitter and receiver, may not necessarily result in improvements in system channel capacity. This emphasizes the importance of considering receiver nonlinearity in the design of communication schemes.

B. 2×2 MIMO System

This section evaluates the impact of the nonlinear characteristics of receivers on the upper and lower bounds of the channel capacity of MIMO systems, and presents numerical results for the channel capacity bounds under two potential channel matrices, $\boldsymbol{h}_1$ and $\boldsymbol{h}_2$

$$\boldsymbol{h}_1 = \begin{bmatrix} 0.9 & 0 \\ 0 & 0.9 \end{bmatrix}, \boldsymbol{h}_2 = \begin{bmatrix} 0.7 & 0.2 \\ 0.3 & 0.6 \end{bmatrix}, \tag{80}$$

where $\boldsymbol{h}_1$ is a diagonal matrix with equal diagonal elements, indicating independent and equivalent signal paths between the receiver and transmitter; while $\boldsymbol{h}_2$ is a non-diagonal matrix, corresponding to transmission signals from multiple transmitters potentially traveling through multiple paths to each receiver, leading to signal interference.

Figures 9(a) and (b) show the relationship between the upper and lower bounds of the channel capacity of a 2×2 MIMO linear receiver system under different noise intensities relative to the peak power constraint A ($\varepsilon = 0.9$). In comparison with Fig. 5, if the receiver "input-output" function is linear, as the allowable peak power increases, the upper and lower bounds grow with $\log_{10} A$, approaching a linear increase at higher values of A.

Figures 10 and 11 show the relationship between the channel capacity and the peak power constraint A for a 2×2 MIMO nonlinear receiver system under different channel matrices $\boldsymbol{h}_1$ and $\boldsymbol{h}_2$, under varying noise conditions.

Clearly, the form of the receiver's nonlinear function significantly affects the trends in MIMO channel capacity. Comparing Figs. 6 and 10, MIMO systems exhibit higher upper and lower bounds of channel capacity than SISO systems. Observing the capacities under channel matrices $\boldsymbol{h}_1$ and $\boldsymbol{h}_2$ in Figs. 10 and 11, it is evident that when there is less interference among the system's transmitting antennas, the upper and lower bounds derived from the channel capacity analysis method proposed in this chapter are tighter and closer to the actual signal capacity. Unlike SISO, the MIMO receiver processes signals from multiple transmitters, enlarging the solution set and increasing the difference between the pre- and post-approximation results. Additionally, since each transmitter adheres to independent power constraints, increasing the number of transmitters leads to greater total transmission power, making it more likely for receivers to operate in nonlinear regions, thus affecting the accuracy of signal reception. This necessitates that OWC system designs fully consider the dynamic range of the channel and the nonlinear characteristics of receivers, guiding the design of transmission signal codebooks based on this.

VI. Conclusion

In this work, we provide a generic OWC model incorporating receiver nonlinearity, background radiated noise, and thermal noise. Our approach is firmly grounded in established information-theoretic methods for capacity analysis. The lower and upper bounds have been derived for SISO and MIMO OWC systems using EPI and dual expression. Numerical results verify the tightness of the derived capacity bounds and highlight the significant relationship between channel capacity and receiver nonlinearity. We believe that as more research emerges on non-monotonic nonlinearities in OWC systems, future experimental studies will likely be able to build on the theoretical foundations established in this work.

Appendix A

Substituting Eqs. (25) and (26) into Eq. (24), we obtain Eq. (81). Via expanding each sub-expression, we have

$$c_1 = -\frac{1}{2}\ln\left(2\pi e\sigma^2\right), \tag{82}$$

$$c_2 = \left[1 - Q\left(-\frac{y}{\sigma}\right)\right]\ln\frac{\sqrt{2\pi e}\sigma}{\rho} + \frac{1}{2}\varpi\left(\frac{y}{\sigma}\right), \tag{83}$$

$$c_3 = \vartheta\left(y\right)\ln\frac{\alpha}{1-\rho}, \tag{84}$$

$$c_4 = Q\left(\frac{\alpha - y}{\sigma}\right)\ln\frac{\sqrt{2\pi e}\sigma}{\rho} + \frac{1}{2}\varpi\left(\frac{\alpha - y}{\sigma}\right), \tag{85}$$

where $Q\left(\cdot\right)$ is the right tail function of the standard normal distribution, defined as

$$Q\left(p\right) = \int_p^\infty \frac{1}{\sqrt{2\pi}} e^{-\frac{x^2}{2}} \mathrm{d}x, \tag{86}$$

and

$$\varpi\left(p\right) = p^2 Q\left(p\right) - \frac{p}{\sqrt{2\pi}} e^{-\frac{p^2}{2}}. \tag{87}$$

It can be proven that $\varpi\left(p\right) < 0$ holds for all $p > 0$.

Therefore, for Eqs. (83) and (85), we have

$$c_2 < \left[1 - Q\left(-\frac{y}{\sigma}\right)\right]\ln\frac{\sqrt{2\pi e}\sigma}{\rho}, \tag{88}$$

$$c_4 < Q\left(\frac{\alpha - y}{\sigma}\right)\ln\frac{\sqrt{2\pi e}\sigma}{\rho}. \tag{89}$$

Inserting the scaled results of these sub-expressions into Eq. (81), it can be proven that Eq. (24) possesses the following

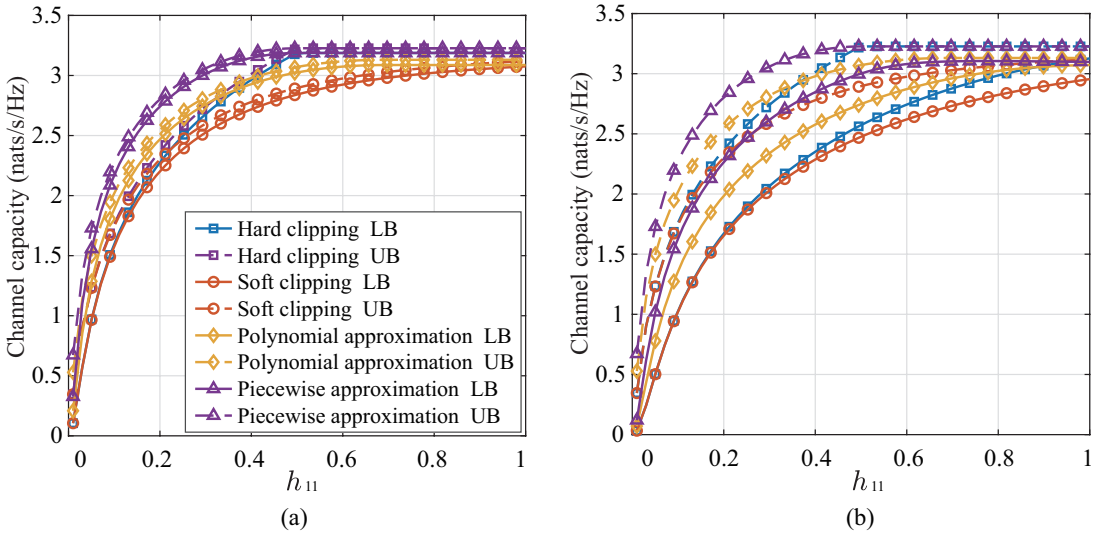

Fig. 8. Upper and lower bounds with respect to h for SISO OWC system with nonlinear receiver. (a) $A = 3$, $\varepsilon = 0.9$, $\sigma = 0.01$. (b) $A = 3$, $\varepsilon = 0.2$, $\sigma = 0.01$.

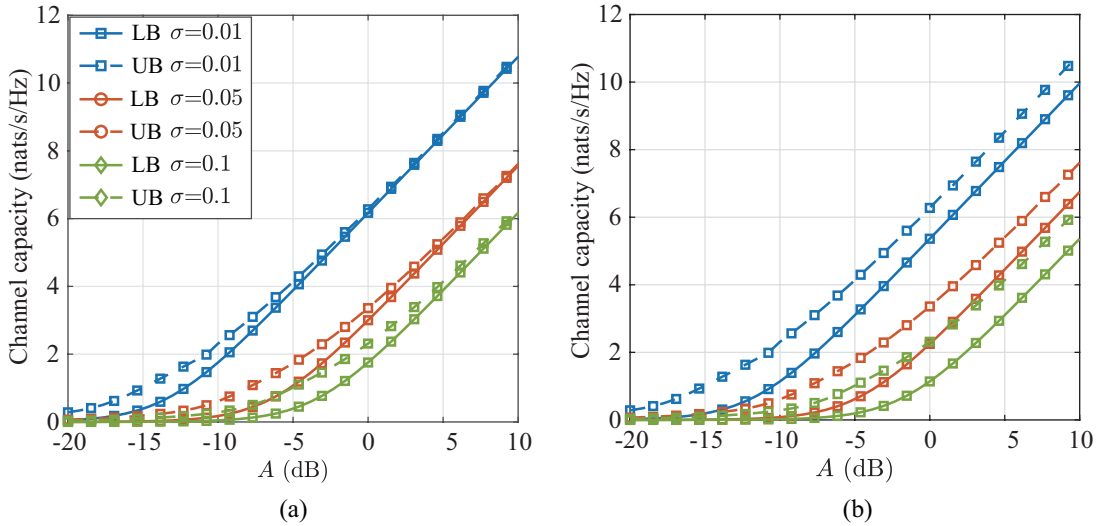

Fig. 9. Upper and lower bounds with respect to A for 2×2 MIMO OWC system with linear receiver ($\varepsilon = 0.9$). (a) $\boldsymbol{h} = \boldsymbol{h}_1$. (b) $\boldsymbol{h} = \boldsymbol{h}_2$.

upper bound

$$\ln \frac{1}{\rho} + \vartheta(y) \ln \frac{\alpha\rho}{\sqrt{2\pi e}\sigma(1-\rho)}. \tag{90}$$

APPENDIX B

Substituting Eqs. (64) and (68) into Eq. (66), we have

$$D\left(P_{\boldsymbol{R}|\boldsymbol{X}}(\boldsymbol{r}|\boldsymbol{x}) \| V_{\boldsymbol{R}}(\boldsymbol{r})\right) = -\ln\left(2\pi e\sigma^2\right) + \int_{-\infty}^{\infty} \frac{1}{(2\pi\sigma^2)^{\frac{M}{2}}} e^{-\frac{\|\boldsymbol{r}-\boldsymbol{\Phi}(\boldsymbol{h}\boldsymbol{x})\|^2}{2\sigma^2}} \ln \frac{1}{V_{\boldsymbol{R}}(\boldsymbol{r})} \mathrm{d}\boldsymbol{r}. \tag{91}$$

When $r_1 \in [0, \alpha_1]$, $r_2 \in [0, \alpha_2]$, $\cdots$, $r_M \in [0, \alpha_M]$, we have Eq. (92).

When r_1, r_2, ,$\cdots$, r_M contain m elements that satisfy $r_i \in [0, \alpha_i]$, with their indices denoted as $S_m(m)$, we have Eq. (93).

Inserting the scaled-down sub-expressions into Eq. (91), it can be easily demonstrated that Eq. (66) is upper bounded by Eq. (70).

REFERENCES

[1] C.-X. Wang, J. Huang, H. Wang, X. Gao, X. You, and Y. Hao, "6G wireless channel measurements and models: Trends and challenges," *IEEE Vehicular Technology Magazine*, vol. 15, no. 4, pp. 22–32, Oct. 2020.

[2] D. Karunatilaka, F. Zafar, V. Kalavally, and R. Parthiban, "LED based indoor visible light communications: State of the art," *IEEE Communications Surveys & Tutorials*, vol. 17, no. 3, pp. 1649–1678, Mar. 2015.

[3] S. Wu, H. Wang, and C.-H. Youn, "Visible light communications for 5G wireless networking systems: From fixed to mobile communications," *IEEE Network*, vol. 28, no. 6, pp. 41–45, Nov. 2014.

[4] C. E. Shannon, "Channels with side information at the transmitter," *IBM Journal of Research and Development*, vol. 2, no. 4, pp. 289–293, Oct. 1958.

[5] A. Lapidoth and S. M. Moser, "On the capacity of the discrete-time Poisson channel," *IEEE Transactions on Information Theory*, vol. 55, no. 1, pp. 303–322, Dec. 2009.

[6] J. Cao, S. Hranilovic, and J. Chen, "Capacity-achieving distributions for the discrete-time Poisson channelpart I: General properties and numerical techniques," *IEEE Transactions on Communications*, vol. 62, no. 1, pp. 194–202, Dec. 2014.

[7] A. Lapidoth, J. H. Shapiro, V. Venkatesan, and L. Wang, "The discrete-

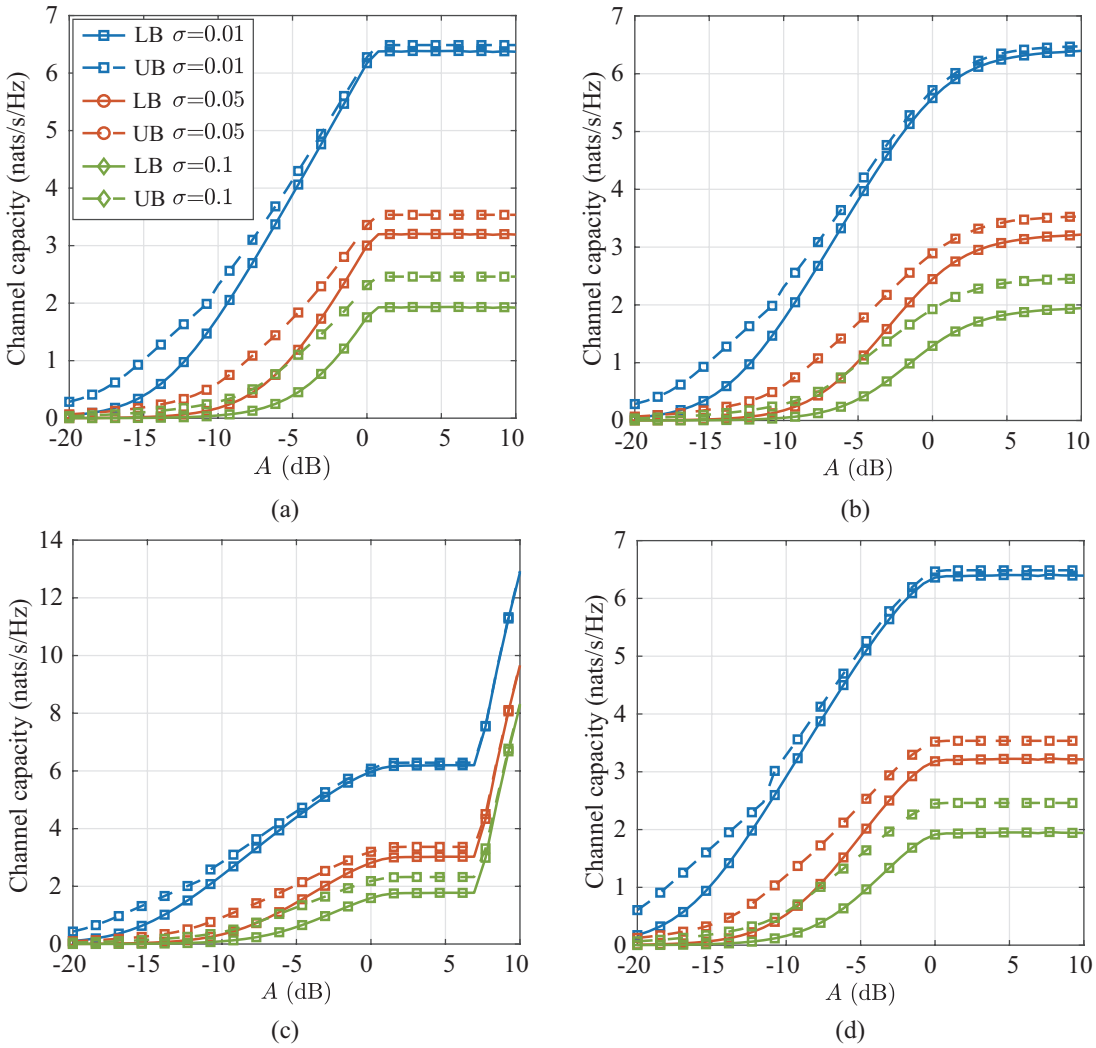

Fig. 10. Upper and lower bounds with respect to A for 2×2 MIMO OWC system with nonlinear receiver ($\boldsymbol{h} = \boldsymbol{h}_1$, $\varepsilon = 0.9$). (a) Hard clipping ($\beta = 1$). (b) Soft clipping ($\beta = 1$, $k = 1$). (c) Polynomial approximation ($\beta_1 = 1.5$, $\beta_2 = -0.75$, $\beta_3 = 0.1$). (d) Piecewise approximation ($\gamma = 1$, $\beta = 1$).

time Poisson channel at low input powers," *IEEE Transactions on Information Theory*, vol. 57, no. 6, pp. 3260–3272, May 2011.

[8] J. Cao, S. Hranilovic, and J. Chen, "Capacity and nonuniform signaling for discrete-time Poisson channels," *Journal of Optical Communications and Networking*, vol. 5, no. 4, pp. 329–337, Apr. 2013.

[9] S. Haas and J. Shapiro, "Capacity of wireless optical communications," *IEEE Journal on Selected Areas in Communications*, vol. 21, no. 8, pp. 1346–1357, Oct. 2003.

[10] J. Pierce, E. Posner, and E. Rodemich, "The capacity of the photon counting channel," *IEEE Transactions on Information Theory*, vol. 27, no. 1, pp. 61–77, Jan. 1981.

[11] M. Davis, "Capacity and cutoff rate for Poisson-type channels," *IEEE Transactions on Information Theory*, vol. 26, no. 6, pp. 710–715, Nov. 1980.

[12] A. Lapidoth, S. M. Moser, and M. A. Wigger, "On the capacity of free-space optical intensity channels," *IEEE Transactions on Information Theory*, vol. 55, no. 10, pp. 4449–4461, Sept. 2009.

[13] A. A. Farid and S. Hranilovic, "Capacity bounds for wireless optical intensity channels with Gaussian noise," *IEEE Transactions on Information Theory*, vol. 56, no. 12, pp. 6066–6077, Nov. 2010.

[14] J.-B. Wang, Q.-S. Hu, J. Wang, M. Chen, and J.-Y. Wang, "Tight bounds on channel capacity for dimmable visible light communications," *Journal of Lightwave Technology*, vol. 31, no. 23, pp. 3771–3779, Oct. 2013.

[15] L. Li, S. M. Moser, L. Wang, and M. Wigger, "On the capacity of MIMO optical wireless channels," *IEEE Transactions on Information Theory*, vol. 66, no. 9, pp. 5660–5682, Mar. 2020.

[16] S. Yang, L. Li, and J. Wang, "High-SNR capacity of MIMO optical intensity channels: A sphere-packing perspective," *IEEE Communications Letters*, vol. 26, no. 10, pp. 2302–2306, Jul. 2022.

[17] D. Falconer, S. Ariyavisitakul, A. Benyamin-Seeyar, and B. Eidson, "Frequency domain equalization for single-carrier broadband wireless systems," *IEEE Communications Magazine*, vol. 40, no. 4, pp. 58–66, Apr. 2002.

[18] H. E. Rowe, "Memoryless nonlinearities with gaussian inputs: Elementary results," *The Bell System Technical Journal*, vol. 61, no. 7, pp. 1519–1525, Sept. 1982.

[19] J. Boccuzzi, "Performance evaluation of non-linear transmit power amplifiers for North American digital cellular portables," *IEEE Transactions on Vehicular Technology*, vol. 44, no. 2, pp. 220–228, May 1995.

[20] E. K. S. Au and W. H. Mow, "Effect of non-linearity on the performance of a MIMO zero-forcing receiver with channel estimation errors," in *Proc. IEEE International Conference on Communications*, 2007, pp. 4150–4155.

[21] M. Sabbaghian, A. I. Sulyman, and V. Tarokh, "Analysis of the impact of nonlinearity on the capacity of communication channels," *IEEE Transactions on Information Theory*, vol. 59, no. 11, pp. 7671–7683, Aug. 2013.

[22] P. Zillmann and G. Fettweis, "On the capacity of multicarrier transmission over nonlinear channels," in *Proc. IEEE 61st Vehicular Technology Conference*, 2005, pp. 1148–1152.

[23] H. Gacanin and F. Adachi, "On capacity of OFDM/TDM using MMSE-FDE in a nonlinear and frequency-selective fading channel," in *Proc. 14th Asia-Pacific Conference on Communications*, 2008, pp. 1–5.

This article has been accepted for publication in IEEE Transactions on Wireless Communications. This is the author's version which has not been fully edited and content may change prior to final publication. Citation information: DOI 10.1109/TWC.2025.3559879

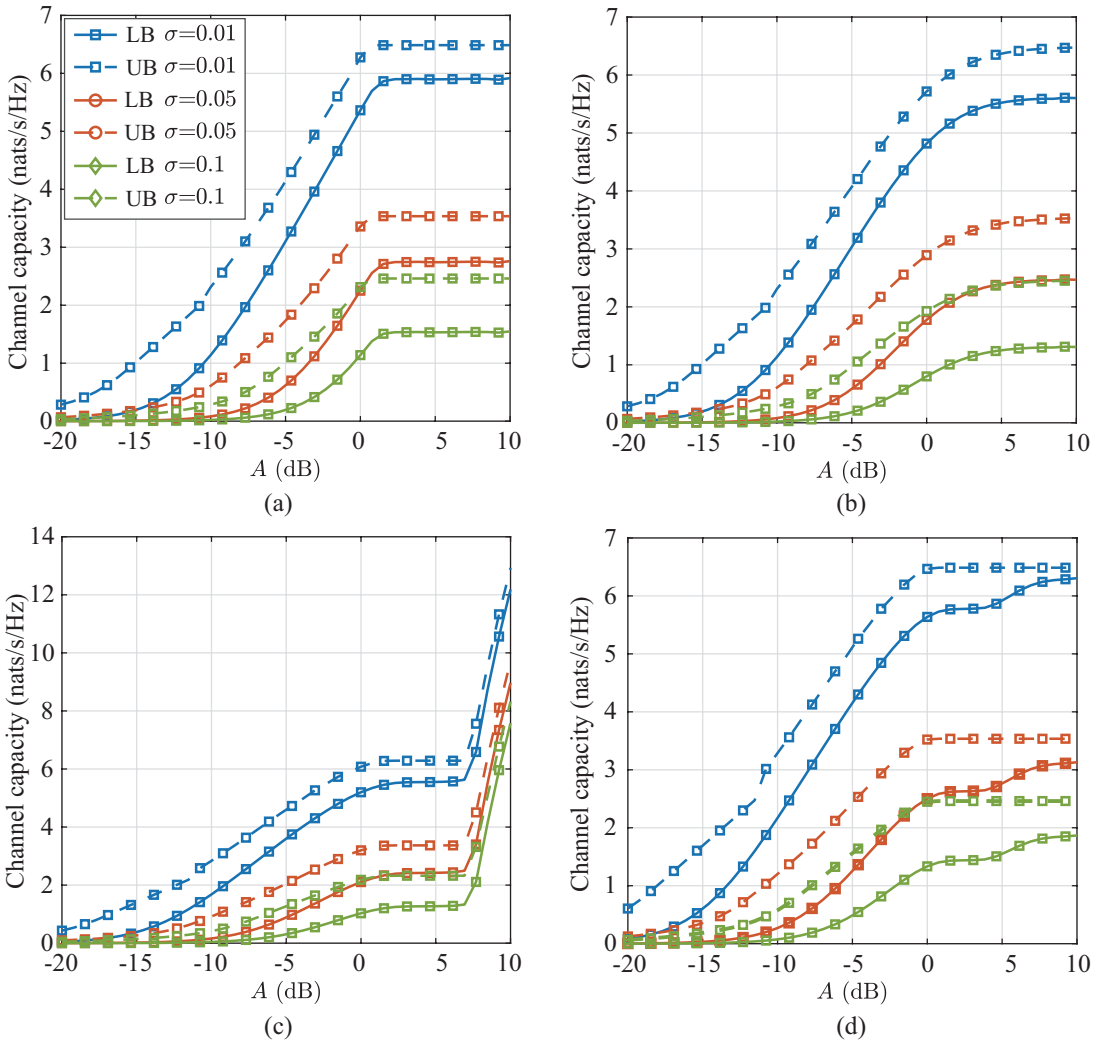

Fig. 11. Upper and lower bounds with respect to A for 2×2 MIMO OWC system with nonlinear receiver ($\boldsymbol{h} = \boldsymbol{h}_2$, $\varepsilon = 0.9$). (a) Hard clipping ($\beta = 1$). (b) Soft clipping ($\beta = 1$, $k = 1$). (c) Polynomial approximation ($\beta_1 = 1.5$, $\beta_2 = -0.75$, $\beta_3 = 0.1$). (d) Piecewise approximation ($\gamma = 1$, $\beta = 1$).

$$
\begin{aligned}
D\left(P_{R|X}\left(r\,|x\right)\|V_R(r)\right) &= \int_{-\infty}^{\infty} \frac{1}{\sqrt{2\pi}\sigma} e^{-\frac{(r-\phi(hx))^2}{2\sigma^2}} \ln\left[\frac{1}{V_R(r)\sqrt{2\pi}\sigma} e^{-\frac{(r-\phi(hx))^2}{2\sigma^2}}\right] \mathrm{d}r \\
&= \underbrace{\int_{-\infty}^{\infty} \frac{1}{\sqrt{2\pi}\sigma} e^{-\frac{(r-\phi(hx))^2}{2\sigma^2}} \ln\left[\frac{1}{\sqrt{2\pi}\sigma} e^{-\frac{(r-\phi(hx))^2}{2\sigma^2}}\right] \mathrm{d}r}_{c_1} + \underbrace{\int_{-\infty}^{0} \frac{1}{\sqrt{2\pi}\sigma} e^{-\frac{(r-\phi(hx))^2}{2\sigma^2}} \ln\left[\frac{\sqrt{2\pi}\sigma}{\rho} e^{\frac{r^2}{2\sigma^2}}\right] \mathrm{d}r}_{c_2} \\
&\quad + \underbrace{\int_{0}^{\alpha} \frac{1}{\sqrt{2\pi}\sigma} e^{-\frac{(r-\phi(hx))^2}{2\sigma^2}} \ln\frac{\alpha}{1-\rho} \mathrm{d}r}_{c_3} + \underbrace{\int_{\alpha}^{\infty} \frac{1}{\sqrt{2\pi}\sigma} e^{-\frac{(r-\phi(hx))^2}{2\sigma^2}} \ln\left[\frac{\sqrt{2\pi}\sigma}{\rho} e^{\frac{(r-\alpha)^2}{2\sigma^2}}\right] \mathrm{d}r}_{c_4}. \qquad (81)
\end{aligned}
$$

$$
\int_{\mathbf{0}}^{\boldsymbol{\alpha}} \frac{1}{\left(2\pi\sigma^2\right)^{\frac{M}{2}}} e^{-\frac{\|\boldsymbol{r}-\boldsymbol{\Phi}(\boldsymbol{h}\boldsymbol{x})\|^2}{2\sigma^2}} \ln \frac{\prod_{j=1}^{M} \alpha_j}{1-\sum_{k=0}^{M-1} \rho_k} \mathrm{d}\boldsymbol{r} = \prod_{i=1}^{M} \vartheta\left(\alpha_i, y_i\right) \ln \frac{\prod_{j=1}^{M} \alpha_j}{1-\sum_{k=0}^{M-1} \rho_k}. \qquad (92)
$$

$$\int_{\boldsymbol{r}_{S_m(n)}} \int_{\widehat{\boldsymbol{r}_{S_m(n)}}} \frac{1}{\left(2\pi\sigma^2\right)^{\frac{M}{2}}} e^{-\frac{\|\boldsymbol{r}-\boldsymbol{\Phi}(\boldsymbol{h}\boldsymbol{x})\|^2}{2\sigma^2}} \ln\left(\frac{\left(2\pi\sigma^2\right)^{\frac{M-n}{2}} \prod_{k=1}^{n} \alpha_{S_n(j,k)} C_M^n}{\rho_n} e^{\frac{\left\|\left|\boldsymbol{r}_{S_n(j)}-\boldsymbol{\alpha}_{S_n(j)/2}\right|-\boldsymbol{\alpha}_{S_n(j)/2}\right\|^2}{2\sigma^2}}\right) \mathrm{d}\boldsymbol{r}$$

$$\leqslant \prod_{p\in S_m(n)} \vartheta\left(\alpha_p, y_p\right) \prod_{q\in\widehat{S_m(n)}} \left[1-\vartheta\left(\alpha_q, y_q\right)\right] \ln \frac{\left(2\pi e\sigma^2\right)^{\frac{M-m}{2}} \prod_{l\in S_m(n)} \alpha_l C_M^m}{\rho_m}. \quad (93)$$

[24] F. Peng and W. E. Ryan, "On the capacity of clipped OFDM channels," in *Proc. IEEE International Symposium on Information Theory*, 2006, pp. 1866–1870.

[25] M. Valkama, A. Shahed hagh ghadam, L. Anttila, and M. Renfors, "Advanced digital signal processing techniques for compensation of nonlinear distortion in wideband multicarrier radio receivers," *IEEE Transactions on Microwave Theory and Techniques*, vol. 54, no. 6, pp. 2356–2366, Jun. 2006.

[26] B. F. Beidas, R. I. Seshadri, and N. Becker, "Multicarrier successive predistortion for nonlinear satellite systems," *IEEE Transactions on Communications*, vol. 63, no. 4, pp. 1373–1382, Feb. 2015.

[27] T. Kübarsepp, A. Haapalinna, P. Kärhä, and E. Ikonen, "Nonlinearity measurements of silicon photodetectors," *Applied Optics*, vol. 37, no. 13, pp. 2716–2722, May 1998.

[28] Y. Li, M. Safari, R. Henderson, and H. Haas, "Nonlinear distortion in SPAD-based optical OFDM systems," in *Proc. IEEE Globecom Workshops (GC Wkshps)*, 2015, pp. 1–6.

[29] S. Huang, Y. Li, C. Chen, M. D. Soltani, R. Henderson, M. Safari, and H. Haas, "Performance analysis of SPAD-based optical wireless communication with OFDM," *Journal of Optical Communications and Networking*, vol. 15, no. 3, pp. 174–186, Feb. 2023.

[30] A. Eisele, R. Henderson, B. Schmidtke, T. Funk, L. Grant, J. Richardson, and W. Freude, "185 MHz count rate 139 dB dynamic range single-photon avalanche diode with active quenching circuit in 130 nm CMOS technology," in *Proc. International Image Sensor Workshop*, 2011, pp. 278–280.

[31] H. Zhang, X. Fan, and E. S. Sinencio, "A low-power, linearized, ultra-wideband LNA design technique," *IEEE Journal of solid-state circuits*, vol. 44, no. 2, pp. 320–330, Jan. 2009.

[32] S. Almonacil, F. Boitier, and P. Layec, "Performance model and design rules for optical systems employing low-resolution DAC/ADC," *Journal of Lightwave Technology*, vol. 38, no. 11, pp. 3007–3014, Apr. 2020.

[33] S. Papoulis, *Probability, Random Variables and Stochastic Processes by Athanasios*. Boston: McGraw-Hill, 2002.

[34] T. M. Cover, *Elements of Information Theory*. John Wiley & Sons, 1999.